Available online at www.sciencedirect.com
ScienceDirect
Journal of Photochemistry and Photobiology A: Chemistry 183 (2006) 212–217
Journal of Photochemistry and Photobiology A:Chemistry
www.elsevier.com/locate/jphotochem

Structural and optical properties of a thiophene-benzobisthiazole derivative

Jun-Gill Kang [a,*], Hyung-Gook Cho [a], Sung Kwon Kang [a], Changmoon Park [a], Sang Woo Lee [b], Gi Beum Park [b], Jong Sook Lee [b], In Tae Kim [b]

[a] *Department of Chemistry, Chungnam National University, Daejeon 305-764, Republic of Korea*
[b] *Department of Chemistry, Kwangwoon University, 447-1 Wolgye-Dong, Nowon-Ku, Seoul 139-701, Republic of Korea*

Received 13 January 2006; received in revised form 6 March 2006; accepted 16 March 2006
Available online 29 March 2006

Abstract

A novel 4,8-bis(2-thiophyl)-2,6-dihexyl-benzo[1,2-d:4,5-d′]bisthiazole (BTDBBT) was synthesized and its crystal structure was determined to be monoclinic, *C*2/*c*, $a = 27.379(6)$ Å, $b = 10.566(2)$ Å, $c = 9.916(2)$ Å, $\beta = 106.49(3)^\circ$, $V = 2750.5(10)$ Å^3, and $Z = 4$. In this structure, the two thiophene moieties lie in almost the same plane as the main benzobisthiazole frame. Absorption, photoluminescence (PL), luminescence, and excitation spectra of BTDBBT are reported. Its structural and optical features were determined using ab initio Hartree–Fock (HF/6-31G**), density functional theory (DFT-B3LYP/6-31G**), and semiempirical (ZINDO) methods.

Keywords: 4,8-Bis(2-thiophyl)-2,6-dihexyl-benzo[1,2-d:4,5-d′]bisthiazole; X-ray structure; Luminescence; Ab initio HF; Semiempirical ZINDO

1. Introduction

Benzobisthiazole derivatives in which organic chromophores are substituted at the 2 and 6 positions have received considerable attention because of their unique photophysical and photochemical properties [1–5]. Typical chromophores used by researchers are phenyl, naphthyl, and anthryl groups. Those compounds expand the π-conjugated system to enhance the intensity of the large red-shift luminescence and increase the rigidity of the molecular unit to inhibit intermolecular photoreactions. Some phenylbenzothiazole derivatives reveal photochromic proton transfer [6] and exhibit highly efficient optical nonlinearities [3]. Previously, we synthesized 4,8-bis(2-thiophyl)-2,6-dihexyl-benzo[1,2-d;4,5-d′]bisthiazole (BTDBBT) and its polymer [7]. To overcome its insolubility in common organic solvents, two hexyl side groups were added to the phenyl ring. Untill now, the structural and optical properties of 4,8-disubstituted benzobisthiazole derivatives have not been reported. For BTDBBT, the 4,8-disubstituted thiophyl groups not only provide π-conjugated electrons, but also add the two lone-paired electrons of sulfur to the molecular unit. However, the steric hindrance between the thiazole moieties and the thiophene frame is expected to destabilize the π resonance. In this study, we obtained X-ray crystallographic and spectroscopic data in order to elucidate the structural and optical properties of 4,8-disubstituted thiophyl derivative. We also performed ab initio calculations for BTDBBT to interpret the observed optical properties. The experimentally observed structural and optical properties of BTDBBT are discussed in terms of the theoretical calculations.

2. Experimental

2.1. Synthesis

4,8-Dibromo-2,6-dihexyl-benzo[1,2-d:4,5-d′]bisthiazole (1 g, 1.93 mmol), 2-trimethylstannylthiophene (1.2 g, 0.48 mmol), and $Pd(PPh_3)_4$ (92 mg, 0.08 mmol, 2 mol%) were weighted in a dry box, and 12 mL of dry toluene and 12 mL of 1 M Na_2CO_3 were put in a two-neck round flask equipped with a stirring bar and a long air condenser capped with a drying tube. The mixture was stirred for 20 h at 90 °C. During the course of the reaction, the reaction mixture turned from pale yellow to dark red. The reaction mixture was cooled and the crude product was extracted using dichloromethane. The organic layer was dried with anhydrous $MgSO_4$ and filtered. The solvent was removed under reduced pressure. The product was recrystallized with hexane

* Corresponding author. Fax: +82 42 821 6548.
E-mail address: jgkang@cnu.ac.kr (J.-G. Kang).

1010-6030/$ – see front matter © 2006 Elsevier B.V. All rights reserved.
doi:10.1016/j.jphotochem.2006.03.023

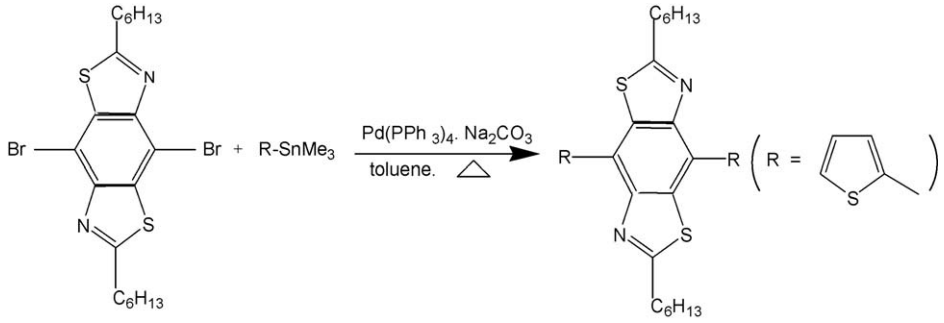

Scheme 1.

to yield BTDBBT. The yield was 82% (0.7 g) and was soluble in common organic solvents such as $CHCl_3$, CH_2Cl_2, and THF. FT-IR (KBr): 3070, 2948, 2921, 2844, 1540, 1453, 1251, 1074, 847, and 690 cm^{-1}. ^1H NMR (in $CDCl_3$): δ7.93(d, 2H), 7.55(d, 2H), 7.25(t, 2H), 3.18(t, 4H), 1.96(m, 4H), 1.61–1.37(m, 12H), 0.92(t, 6H). ^{13}C NMR (in $CDCl_3$): δ172.3, 133.9, 128.4, 127.5, 126.8, 121.4, 77.4, 77.0, 76.6, 34.5, 31.5, 29.3, 28.8, 22.5, 14.1. λ_{max}(in $CHCl_3$): = 370 nm; HRMS calc. for $C_{28}H_{33}N_2S_4$ *m/z* 525.1527, found 525.1502 (Scheme 1).

2.2. X-ray crystallography

Intensity data were collected at room temperature on a Bruker SMART CCD diffractometer using graphite monochromated Mo Kα radiation. The structure of the titled compound was solved by applying the direct method using a SHELXS-97 and refined by a full-matrix least-squares calculation on F^2 using SHELXL-97 [8]. All non-H atoms were refined an isotropically. All hydrogen atoms were calculated in ideal positions and were riding on their respective carbon atoms ($B_{iso} = 1.2B_{eq}$ and $1.5B_{eq}$). The crystal data and refinement results are summarized in Table 1.

2.3. Molecular modeling

The geometry of BTDBBT was optimized on the level of both HF/6-31G, HF/6-31G(d,p)**, DFT-B3LYP/6-31G, and DFT-B3LYP/6-3G(d,p)** using Gaussian 03 [9]. The electronic structure and optical properties were also determined using the semiempirical (ZINDO) method.

2.4. Spectroscopic measurements

For low-temperature photoluminescence (PL), luminescence, and excitation spectra, a powdered sample was placed on the cold finger of a CTI-cryogenics using silicon grease. The sample was irradiated with an He–Cd 325-nm laser line or the light from an Oriel 1000 W Xe lamp (working power, 600 W) after it passed through an Oriel MS257 monochromator. The spectra were measured at 90° angle with an ARC 0.5 m Czerny–Turner monochromator equipped with a cooled Hamamatsu R-933-14 PM tube.

Table 1
Crystal data and structure refinement for BTDBBT

Empirical formula	C28 H32 N2 S4
Formula weight	524.80
Temperature	293(2) K
Wavelength	0.71073 Å
Crystal system, space group	Monoclinic, *C*12/*c*1
Unit cell dimensions	*a* = 27.379(6) Å, alpha = 90°. *b* = 10.566(2) Å, beta = 106.49(3)°. *c* = 9.916(2) Å, gamma = 90°.
Volume	2750.5(10) $Å^3$
Z, calculated density	4, 1.267 Mg/m^3
Absorption coefficient	0.365 mm^{-1}
F (0 0 0)	1112
Crystal size	0.4 mm × 0.4 mm × 0.1 mm
Theta range for data collection	1.55–27.50°
Limiting indices	$-35 \le h \le 35$, $-13 \le k \le 13$, $-12 \le l \le 12$
Reflections collected/unique	12825/3156 [R(int) = 0.0278]
Completeness to theta = 27.50	99.9%
Absorption correction	Empirical
Maximum and minimum transmission	0.945 and 0.844
Refinement method	Full-matrix least-squares on F^2
Data/restraints/parameters	3156/3/154
Goodness-of-fit on F^2	1.098
Final *R* indices [$I > 2\sigma(I)$]	$R_1 = 0.0592$, w$R_2 = 0.1735$
R indices (all data)	$R_1 = 0.0906$, w$R_2 = 0.2135$
Largest differential peak and hole	0.827 and −0.440 e$Å^{-3}$

3. Results and discussion

3.1. X-ray crystallographic analysis

BTDBBT crystallizes in the monoclinic space group *C*2/*c*. A perspective view of the molecular structure of BTDBBT with the atomic numbering scheme is shown in Fig. 1 and the bond distances and bond angles are listed in Table 2. The X-ray crystal structure shows that the two thiophene moieties lie almost planar to the main benzobisthiazole frame. In the near planar structure, the steric hindrance between the thiophene moieties and benzobisthiazole frame is expected to be large and unfavorable energetically. The observed dihedral angle between them is only 21°. This suggests that the advantages in both the crystal stacking effect and the electronic resonance effect of the molecule may

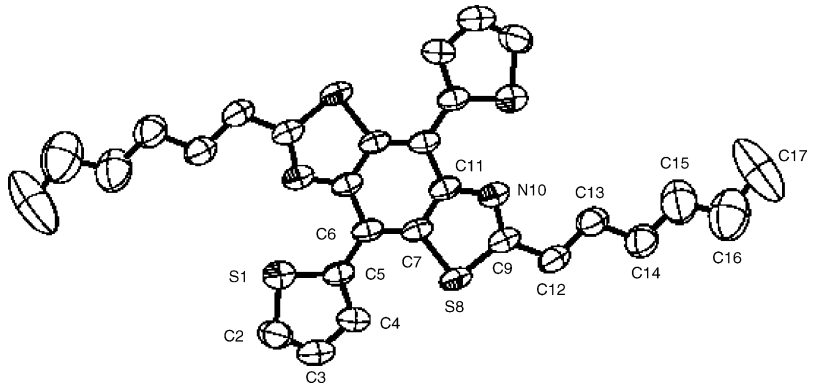

Fig. 1. View of BTDBBT showing atom labeling and ellipsoids at 50%. In this view, hydrogen atoms are omitted for clarity.

overcome the unfavorable steric hindrance between the thiazole moieties and bisthiophene frame.

3.2. Absorption, luminescence, and excitation spectra

Fig. 2(a) shows the absorption spectra of BTDBBT dissolved in CH_2Cl_2. Two characteristic bands appeared in the UV–vis region: a very broad band ($\lambda_{max} = 362$ nm, $\varepsilon = 23{,}600\ M^{-1}\ cm^{-1}$) and a sharp band ($\lambda_{max} = 288$ nm, $\varepsilon = 19{,}390\ M^{-1}\ cm^{-1}$). In addition, a weak band appeared at 250 nm. Hereafter, these three bands will be referred to in order of increasing energy as the A-, B-, and C-bands, respectively. Fig. 3 shows the PL spectrum of BTDBBT in CH_2Cl_2 solution measured at room temperature. The PL spectrum has two main components, peaking at 425 and 440 nm, with the shoulder at the low-energy side. This multicomponent structure could be related with the vibronic structure. The luminescence and excitation spectra of BTDBBT in solid state were measured at 10 K to reveal the correlation between the luminescence property and the molecular structure in details. As shown in Fig. 4(a), for the solid state at low-temperature, the luminescence spectrum was split

Table 2
Bond lengths (Å) and angles (°) for BTDBBT

S(1)–C(2)	1.700(4)	S(1)–C(5)	1.716(4)
C(2)–C(3)	1.333(6)	C(3)–C(4)	1.423(6)
C(4)–C(5)	1.421(4)	C(5)–C(6)	1.469(4)
C(6)–C(7)	1.397(5)	C(6)–C(11) #1	1.419(4)
C(7)–C(11)	1.410(4)	C(7)–S(8)	1.749(3)
S(8)–C(9)	1.744(4)	C(9)–N(10)	1.304(4)
C(9)–C(12)	1.505(5)	N(10)–C(11)	1.393(4)
C(11)–C(6) #1	1.419(4)	C(12)–C(13)	1.499(5)
C(13)–C(14)	1.504(6)	C(14)–C(15)	1.511(6)
C(15)–C(16)	1.486(7)	C(16)–C(17)	1.505(8)
C(2)–S(1)–C(5)	92.2(2)	C(3)–C(2)–S(1)	112.9(3)
C(2)–C(3)–C(4)	113.8(3)	C(5)–C(4)–C(3)	110.6(3)
C(4)–C(5)–C(6)	126.5(3)	C(4)–C(5)–S(1)	110.5(3)
C(6)–C(5)–S(1)	123.0(2)	C(7)–C(6)–C(11) #1	113.8(3)
C(7)–C(6)–C(5)	124.3(3)	C(11) #1–C(6)–C(5)	122.0(3)
C(6)–C(7)–C(11)	123.8(2)	C(6)–C(7)–S(8)	128.1(2)
C(11)–C(7)–S(8)	108.1(2)	C(9)–S(8)–C(7)	89.78(15)
N(10)–C(9)–C(12)	123.5(3)	N(10)–C(9)–S(8)	115.7(3)
C(12)–C(9)–S(8)	120.7(2)	C(9)–N(10)–C(11)	110.6(3)
N(10)–C(11)–C(7)	115.7(2)	N(10)–C(11)–C(6) #1	121.8(3)
C(7)–C(11)–C(6) #1	122.4(3)	C(13)–C(12)–C(9)	114.7(3)
C(12)–C(13)–C(14)	114.0(3)	C(13)–C(14)–C(15)	112.1(4)
C(16)–C(15)–C(14)	119.0(6)	C(15)–C(16)–C(17)	108.5(7)

Symmetry transformations used to generate equivalent atoms: #1 $-x+1/2$, $-y+3/2$, $-z$.

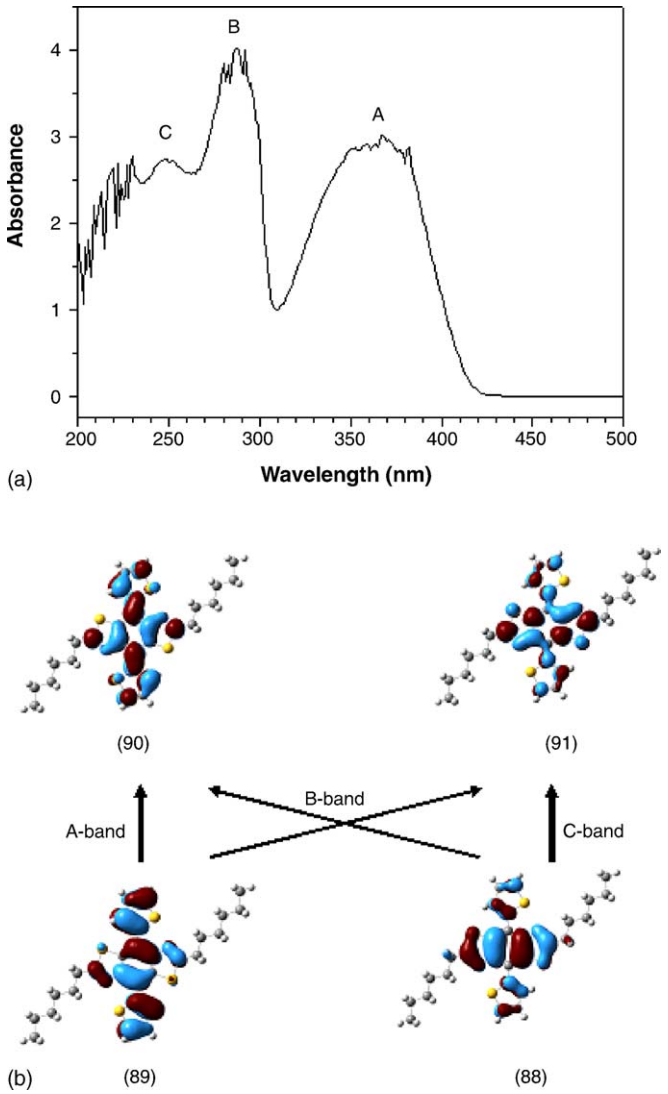

Fig. 2. (a) Absorption spectrum of BTDBBT dissolved in $CHCl_3$ (concentration = 1.33×10^{-4} M) and (b) predominant HF molecular orbitals responsible for the A-, B-, and C-absorption bands.

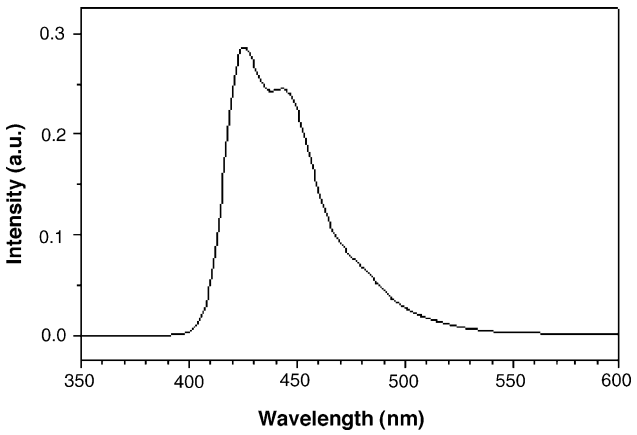

Fig. 3. PL spectrum of BTDBBT dissolved in $CHCl_3$, excited by a 325-nm He–Cd laser line (concentration = 7.6×10^{-5} M).

well and the intensity was enhanced significantly. The spectrum of the solid sample was also red-shifted by more than 100 nm, compared with that of the solution state. As shown in Fig. 4(b), the excitation spectrum was very broad, ranging from 250 to 500 nm. The excitation spectrum of the solid state was unexpectedly uncharacteristic, but could be resolved into two parts.

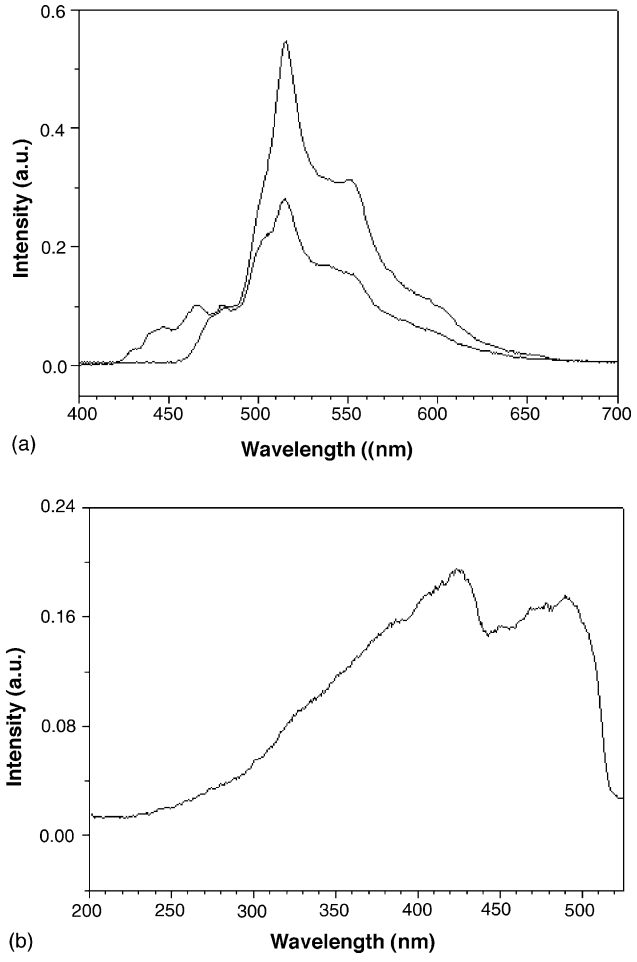

Fig. 4. (a) Emission (upper: $\lambda_{exc} = 470$ nm, lower: $\lambda_{exc} = 372$ nm) and (b) excitation ($\lambda_{ems} = 550$ nm) spectra of BTDBBT in solid state at 10 K.

Considering the red-sift for the solid states, the low-energy part, peaking at 480 nm, corresponded to the A-absorption band. The high-energy part was very broad, ranging from 250 to 430 nm. The 420-nm peak component and the long tail at the high-energy shoulder corresponded to the B- and C-absorption bands, respectively.

3.3. Structural calculation and assignments

The structural calculation provided useful information about the electronic structures and electronic transitions of the model molecule. We also performed ab initio calculation for BTDBBT to reveal the resonance effect and interpret the observed optical properties. The initial structure, which had been built using X-ray crystallographic data, was optimized on the level of DFT-B3LYP/6-31G both HF/6-31G** and DFT-B3LYP/6-31G** using Gaussian 03 [9]. Starting from the optimized conformations, the dihedral angle ϕ between the benzobisthiazole frame and the one-side thiophene moiety on the side and $-\phi$ for the other part were rotated from 0° to 180° in 10° increments. The calculated rotational energies for the free BTDBBT on the level of both HF/6-31G and DFT-B3LYP/6-31G, with and without polarization functions, allowed the selection of a preferred conformation. The dihedral angle between the benzobisthiazole frame and the thiophene moiety was found to be 21° from the X-ray crystal structure. As shown in Fig. 5, the results of DFT quantum mechanical calculations on the level of B3LYP/6-31G//B3LYP/6-31G(d,p) found a global minimum at $\phi = 30°$. This value was very close to that of the X-ray crystal structure. In the near planar structure, the steric hindrances within the molecule become very unfavorable energetically. However, the results of DFT calculations at the level of B3LYP/6-31G//B3LYP/6-31G(d,p) implied that the electronic resonance effect of the molecule in such a planar structure

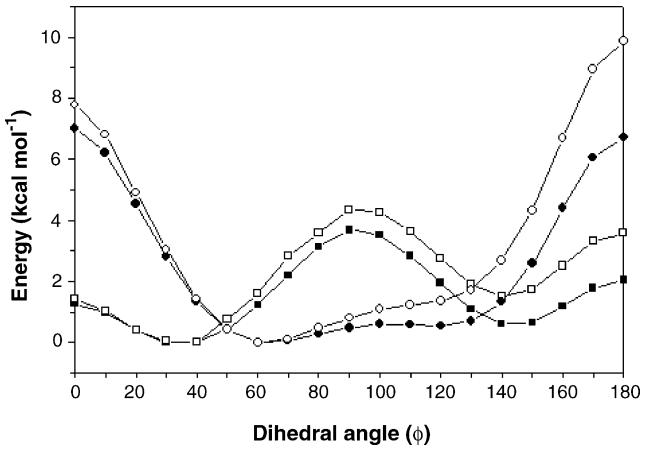

Fig. 5. Rotational energy barrier between the center and two neighboring thiophenes. Each point for the relative dihedral angle ϕ indicates the relative potential energy for the optimized BTDBBT with fixed ϕ for S23-C29-C32-C37 and $-\phi$ for S44-C38-C35-C30. Solid and open square, and solid and open circle symbols represent the optimized values, using DFT-B3LYP/6-31G, DFT-B3LYP/6-31G(d,p)**, HF/6-31G, and HF/6-31G(d,p)** methods, respectively. Each energy calculation is done on the optimized structure on the level of DFT-B3LYP/6-31G using Gaussian 03.

overcame the unfavorable steric hindrances between the benzobisthiazole and thiophene parts of the molecule. For the level of HF/6-31G**, in which the resonance effect was not considered, the global minimum reached $\phi = 60^\circ$. Furthermore, the crystal stacking effect results in an advantage in forming the near planar geometry.

Next, using the optimized structure, the electronic structures and electronic transitions for the X-ray crystal structure were calculated on the level of ZINDO using Gaussian 03. The optimized geometry of BTDBBT conforms to C_i symmetry. The results of the molecular orbital (MO) calculations are listed in Table 3. Here, the C_i axis is considered the z-axis. The π-bonding orbitals of benzobisthiazole and the two thiophene moieties became high-energy bonding orbitals. The highest-occupied-molecular orbital (HOMO), 89, was comprised of the π-characters of the carbon atoms in the benzobisthiazole frame and the thiophene moieties. The next two lower HOMOs, 88 and 87, corresponded to the π-orbitals mostly formed from the benzobisthiazole frame and the thiophene moieties, respectively. For 88, the contribution of the sulfur atoms in the benzobisthiazole frame was as much as 37.6%. For the fourth HOMO, 86, all atoms in the benzobisthiazole frame and the thiophene moieties participated in the formation of the π-orbital. The fifth HOMO, 85, is composed mostly of the π-character of the carbon and sulfur atoms in the thiophene moiety, with minor contributions from the nitrogen atom in the benzobisthiazole frame.

Based on the calculated ZINDO results, the three absorption bands of BTDBBT were assigned. As listed in Table 4, the transitions from the X^1A_g ground to any ^1A_g states were forbidden by the parity selection rule, so that the excited ^1A_g states were ruled out. The lowest ungerude-singlet-excited-state (LUSES), 1^1A_u, arose mostly from the transitions from 89 to 90. The calculated oscillator strength, f, of the transition from the X^1A_g ground state to this first excited state was 0.92. This value was the largest among the 20 calculated singlet excited states.

Table 3
Some molecular orbitals calculated for X-ray BTDBBT

No.	Hartree	% Contribution from each part of the complex				
		Bisthiazole			Thiophenes	
		C	N	S	C	S
95	0.067	59.5	19.4	0	21.1	0
94	0.051	58.4	6.8	0	34.8	0
93	0.033	45.0	25.6	0	29.4	0
92	0.015	31.6	7.4	2.2	54.8	4.0
91	0.006	74.7	7.7	5.5	12.1	0
90	−0.020	61.0	0	0	39.0	2.8
89	−0.253	45.7	3.4	0	50.9	0
88	−0.290	51.1	5.4	37.6	5.9	0
87	−0.294	9.3	0	0	90.7	0
86	−0.343	30.5	7.0	19.3	48.1	2.2
85	−0.348	0	15.3	0	35.6	49.1
84	−0.352	7.6	8.7	4.8	29.1	49.8
83	−0.369	9.9	59.5	4.4	15.0	11.2
82	−0.377	15.3	59.0	5.6	12.2	7.9
81	−0.391	21.1	56.4	17.7	0	4.8

Table 4
CI singlet excited states and predominant transitions of BTDBBT

Excited state	eV	Oscillator strength, f	Main transitions
$1A_u$	3.12	0.92	89 → 90
$2A_u$	3.44	0.02	89 → 91
$1A_g$	3.78	0.0	89 → 92
$3A_u$	3.83	0.75	88 → 90; 88, 89 → 91
$2A_g$	4.29	0.0	83 → 93; 82 → 91; 83 → 93
$4A_u$	4.29	0.02	83 → 91, 90; 82 → 93
$3A_g$	4.47	0.0	89 → 93
$5A_u$	4.53	0.11	88 → 91
$4A_g$	4.53	0.0	87 → 90
$6A_u$	4.75	0.04	89 → 94
$7A_u$	4.79	0.01	89 → 96
$5A_g$	4.86	0.0	88 → 92
$8A_u$	5.0	0.03	89 → 95

Accordingly, the strong A-absorption band could be attributed to the $X^1A_g \rightarrow 1^1A_u$ transition. This transition was associated with the π → π* of both the benzobisthiazole frame and thiophene moieties. The second LUSES, $2A_u$, arose mostly from the electronic transitions from 89 to 91. The probability of the $X^1A_g \rightarrow 2^1A_u$ transition was very small with $f = 0.02$ and this transition may have been buried in the A-absorption band. The third LUSES, 3^1Au, resulted predominantly from the transitions from 88 to 90, together with those from 89 to 91 and from 88 to 91. The oscillator strength of the $X^1A_g \rightarrow 3^1A_u$ transition was the second largest with $f = 0.75$. These transitions could be associated with the strong B-absorption band. As listed in Table 4, the contribution indicated that the B-absorption band was associated, in the main, with the π → π* of the benzobisthiazole frame. The next LUSES resulted from the transitions from 83 to 90 and 91, and from 82 to 92 and 93. For MOs 82 and 83, the contribution of the nitrogen atom was exceptionally large, while for MOs 90–93 its contribution was negligible. Accordingly, the oscillator strength of the $X^1A_g \rightarrow 4^1A_u$ transition was very small. As indicated in Table 4, the $X^1A_g \rightarrow 5^1A_u$ transition resulted in the third largest oscillator strength with $f = 0.11$. The 5^1A_u SES arose mostly from the electronic transitions from 88 to 91. The C-absorption band could be attributed to this transition, associated with the π → π* of the benzobisthiazole frame. The predominant orbital transitions involved in the A, B, and C-absorption bands are illustrated in Fig. 2(b).

The observed emission was strongly associated with the 1^1A_u excited state. The A-band excitation, peaking at 470 nm, underwent relaxation to the low vibrational sublevels of the 1^1A_u state, followed by radiative transition from the low sublevels to the ground state. The Stoke's shift was ca. 0.2 eV (1613 cm^{-1}). As seen in the excitation and emission spectra, the emissions produced via the B- and C-band excitations were exactly the same as that via the A-band excitation. This indicates that the populations of the 3^1A_u and the 5^1A_u excited states, gained via the B- and C-band excitations, respectively, could be transfered to the 1^1A_u excited state non-radiatively via the intersystem crossing mechanism. Accordingly, the emission from BTDBBT can be attributed to the π* → π of both the benzobisthiazole frame and thiophene moieties.

4. Conclusion

The crystal structure and optical properties of BTDBBT have been revealed. The X-structure confirms that the benzobisthiazole frame and thiophene moieties form a nearly planar geometry. The DFT quantum mechanical calculation indicates that the electronic resonance effect of the molecule overcomes the steric hindrances between benzobisthiazole and thiophene parts of the molecule. The HOMO and LUMO are comprised of the π-characters of the carbon atoms in the benzobisthiazole frame and the thiophene moieties. The electronic transitions between these two orbitals are associated with strong absorption and luminescence properties of BTDBBT.

5. Supplementary data

Crystallographic data for the structure analysis of 4,8-bis(2-thiophyl)-2,6-dihexyl-benzo[1,2-d:4,5-d′]bisthiazole has been deposited at the Cambridge Crystallographic Data Center and allocated the deposition number CCDC 286763. Copy of the data can be obtained free of charge via www.ccdc.cam.ac.uk/conts/retrieving.html (or from the Cambridge Crystallographic Data Centre, 12, Union Road, Cambridge CB2 1EZ, UK; fax: +44 1223 336033).

Acknowledgements

This work was partly supported by a research grant of Kwangwoon University (2005) and by the Ministry of Information and Communication (MIC), Korea, under the Information Technology Research Center (ITRC) Support Program supervised by the Institute of Information Technology Assessment (IITA) (IITA-2005-C1090-0502-0038).

References

[1] J.F. Wolfe, B.H. Lee, F.E. Arnold, Macromolecules 14 (1981) 915.
[2] J.F. Wolfe, B.H. Loo, Macromolecules 29 (1996) 2783.
[3] S.-H. Lee, A. Otomo, T. Nakahama, T. Yamada, T. Kamikodo, S. Yokoyama, S. Mashiko, Mater. Commun. 12 (2002) 2187.
[4] T. Sasaki, T. Inoue, Y. Komori, S. Irie, K. Sakurai, K. Tsubakiyama, Phys. Chem. Chem. Phys. 5 (2003) 1381.
[5] Y.-H. So, S.J. Martin, B. Bell, C.D. Pfeiffer, R.M. Van Effen, B.L. Romain, S.M. Lefkowitz, Macromolecules 36 (2003) 4699.
[6] (a) R.S. Becker, C. Lenoble, A. Zein, J. Phys. Chem. 91 (1987) 3509;
(b) P.-T. Chou, W.C. Cooper, J.H. Clements, S.L. Studer, C.P. Chang, Chem. Phys. Lett. 216 (1993) 300.
[7] I.T. Kim, S.W. Lee, S.Y. Kim, J.S. Lee, G.B. Park, S.H. Lee, S.K. Kang, J.-G. Kang, Synth. Met. 156 (2006) 38.
[8] G.M. Sheldrick, SHELXS-97 and SHELXL-97. Program for the Refinement of Crystal Structures, University of Göttingen, Germany, 1997.
[9] M.J. Frisch, G.W. Trucks, H.B. Schlegel, G.E. Scuseria, M.A. Robb, J.R. Cheeseman, V.G. Zakrzewski, J.A. Montgomery Jr., T. Vreven, K.N. Kudin, J.C. Burant, J.M. Millam, S.S. Iyengar, J. Tomasi, V. Barone, B. Mennucci, M. Cossi, G. Scalmani, N. Rega, G.A. Petersson, H. Nakatsuji, M. Hada, M. Ehara, K. Toyota, R. Fukuda, J. Hasegawa, M. Ishida, T. Nakajima, Y. Honda, O. Kitao, H. Nakai, M. Klene, X. Li, J.E. Knox, H.P. Hratchian, J.B. Cross, C. Adamo, J. Jaramillo, R. Gomperts, R.E. Stratmann, O. Yazyev, A.J. Austin, R. Cammi, C. Pomelli, J.W. Ochterski, P.Y. Ayala, K. Morokuma, G.A. Voth, P. Salvador, J.J. Dannenberg, V.G. Zakrzewski, S. Dapprich, A.D. Daniels, M.C. Strain, O. Farkas, D.K. Malick, A.D. Rabuck, K. Raghavachari, J.B. Foresman, J.V. Ortiz, Q. Cui, A.G. Baboul, S. Clifford, J. Cioslowski, B.B. Stefanov, G. Liu, A. Liashenko, P. Piskorz, I. Komaromi, R.L. Martin, D.J. Fox, T. Keith, M.A. Al-Laham, C.Y. Peng, A. Nanayakkara, M. Challacombe, P.M.W. Gill, B. Johnson, W. Chen, M.W. Wong, C. Gonzalez, J.A. Pople, Gaussian 03, Revision C.02, Gaussian Inc., Wallingford, CT, 2004.